# Supplementary Information

## Materials and Methods

All chemicals, unless otherwise specified, were obtained from Sigma (St. Louis, MO) or Fisher Scientific (Hampton, NH).

### Purification of proteins

The expression, purification and characterization of F33Y-$Cu_B$Mb variants were performed as described in previous publications.[1]

### Stopped-flow UV-Vis electron transfer rate measurements

Experiments were performed on an Applied Photophysics Ltd. (Leatherhead, U.K.) SX18.MV stopped-flow spectrometer equipped with a 256 element photodiode array detector. Two-syringe mixing was employed to mix equal volumes of 6 μM ferric F33Y-$Cu_B$Mb variants with a solution of 1 mM TMPD and 10 mM ascorbate. All reported data sets originally consisted of 200 spectra collected over 100 s using logarithmic sampling. The integration period and minimum sampling period were both 1 ms. A water bath, connected to the syringe compartment and set to 25ºC, provided temperature control. The actual temperature in the syringe compartment was measured to be 24.4ºC. The instrument was prepared for anaerobic stopped-flow by rinsing its lines out several times with buffer that had been degassed by bubbling argon gas through it. Special glass outer syringes fit with Teflon stoppers into which an argon line was run maintained an oxygen free environment. The ferric protein was degassed on schlenk line and transferred to anaerobic glovebag before being taken to stopped-flow apparatus in a degassed syringe. The TMPD/ascorbate solution was prepared inside the glovebag and transferred onto the stopped-flow using a degassed syringe.

### Oxygen binding affinity and CO recombination measurements

The affinity for $O_2$ was determined using the Flow-Flash technique with a setup described previously[2]. In short, the samples were prepared in modified Thunberg cuvettes (5-30 μM protein, 100 mM phosphate buffer, pH 6). Increased protein

concentrations were needed for F33Y-$Cu_B$Mb (MF heme) and F33Y-$Cu_B$Mb (DF heme) since absorbance maxima of the ferrous state and the ferrous CO bound state were relatively close in wavelength (Fig. S2 C&D). The samples were made anaerobic with $N_2$(g) on a vacuum line and reduced by addition of 100 µM dithionite. The cuvettes were put under 1.5 bar CO(g) and then incubated overnight at 4°C. For Flow-Flash measurements a sample was transferred to a stopped-flow syringe that was pre-incubated with 100 mM dithionite and washed with anaerobic water. The second syringe contained oxygenated buffer (100 mM KPi, pH 6) at $O_2$ concentrations ranging from 0.25 – 1.2 mM. The solution of the two syringes were mixed in a ratio of 1:5 (protein sample/oxygenated buffer) using a custom-built stopped-flow apparatus (Applied Photophysics, U.K.). After mixing (200 ms delay) CO was dissociated by a short laser flash (10 ns, 200 mJ, 523 nm, Nd-YAG laser, Quantel). $O_2$ binding kinetics was then studied at different selected wavelengths by a spectrophotometer and recorded on a digital oscilloscope. The obtained kinetic traces were converted to absorbance changes and the number of points was reduced from $10^6$ to $2*10^3$ averaging over a logarithmic time scale. The traces were then fitted to a model of consecutive irreversible reactions using the software package ProK (Applied Photophysics, U.K.).

CO recombination measurements were performed just before $O_2$ binding affinity experiments on the same samples. After gas exchange for 1.5 bar CO(g), CO recombination was studied at different selected wavelengths. Data recording and processing was performed in the same fashion as for $O_2$ binding affinity experiments.

**Data analysis and fitting**

$O_2$ binding to the F33Y-$Cu_B$Mb variants was measured after CO photolysis in a Flow-Flash experiment. Because of the different optical spectra for each construct, different wavelengths were chosen in order to achieve a good signal. Figure S4 shows $O_2$ binding at 1 mM in the different samples, and Figure S7 shows the data normalized to the same amplitudes in order to emphasize the difference in rate constants for $O_2$ binding observed. Because there were clear differences in the rate constants observed (Fig. S4), with the $O_2$ binding rates increased for those models that have a higher reduction potential, we also studied these rate constants as a function of $O_2$ concentrations (Fig. S5). We also observed in all constructs that $O_2$ binding kinetics is

biphasic with a fast phase of unknown origin, with relatively small contribution to the total absorbance change. The fast phase is more obvious in the models containing the MF- and DF-heme. This biphasic character in the MF- and DF-heme containing models is not explained by residual protein that still contains the wildtype heme, since the rate constants of the slow phase observed in the MF/DF-heme containing models does not match the corresponding rate constant seen in F33Y-$Cu_B$Mb. Since the contribution of the fast phase is in general relatively low, we fitted the complete reaction to only one phase. The rates from these one-exponential fits were then plotted (Fig. S5) and used for calculation of $O_2$ binding properties.

**DFT calculations and analysis**

To help understand the effect of porphyrin substituent on $O_2$ dissociation in HCO, quantum chemical calculations were performed on three $O_2$ bound heme models: heme *b*, MF-heme and DF-heme, in which all porphyrin substituents are kept the same as in the real systems except that the propionate group is replaced by methyl to facilitate the calculations, see Figure S6. The geometries were fully optimized by using the DFT method mPWVWN[3, 4] with a Watcher's basis for Fe,[5] 6-311++G(2d,2p) for all coordinated atoms plus the $O_2$ molecule, and a 6-31G(d) basis for the rest, which was previously found to yield excellent predictions for similar heme protein model systems.[6, 7] Both the closed-shell singlet ferrous oxy ($Fe^{2+}$-$O_2$) and open-shell singlet ferric superoxy ($Fe^{3+}$-$O_2^-$) states were investigated. The atomic charges and spin densities were also calculated. All calculations were performed using the Gaussian 09 program. [8]

As shown in Figure S6, the optimized molecular structures look similar. However, the superoxy form has a relatively longer Fe-$O_2$ bond and slightly longer $O_b$-$O_t$ bond ($O_b$ and $O_t$ are the bridging and terminal oxygen atoms in Fe-$O_2$), see Table S3. The spin density results listed in Table S3 from both Mulliken analysis and Natural Population Analysis (NPA) clearly show the expected spin state patterns: zero spin densities for the oxy form, and an anti-ferromagnetic coupling between iron and $O_2$ moiety for the superoxy form. The energy results indicate that for these three heme systems, the superoxy form is more favorable than the oxy form, consistent with previous reports of oxymyoglobin which show that the Pauling type closed-shell singlet $^1Fe^{II}$-$^1O_2$ is of higher energy than the Weiss type open-shell singlet $^2Fe^{III}\uparrow\downarrow{}^2O_2^-$.[9, 10, 11, 12, 13, 14]

However, the small energy differences of ~ 2 kcal/mol in all these heme systems suggest that with a little activation energy, the system can move to the oxy form, which has a formally neutral $O_2$ moiety, close to the $O_2$ dissociated state. In fact, both Mulliken charges and NPA charges of all these complexes exhibit the same trend that the $O_2$ fragment has a less negative or closer to neutral charge in the oxy form than the superoxy form, see Table S3. Moreover, it is interesting to note that e.g. Mulliken charges of $O_2$ fragment in the oxy form follows a trend of heme b (-0.051 e) < MF-heme (-0.044 e) < DF-heme (-0.034 e). Even the superoxy form's $O_2$ fragment charge becomes less negative with more electron-withdrawing substituent. This suggests that with more electron-withdrawing substituents on porphyrin or higher redox potential, it helps attract the negative charge from $O_2$ fragment back to iron porphyrin as exemplified by less positive iron charges in Table S3, which makes $O_2$ even closer to a neutral state and thus more prepared for dissociation. This trend is consistent with the observed experimental $O_2$ dissociation rates in these hemes. The charges calculated using a different theoretical approach (NPA) also display the same trend (see Table 1, S3), further supporting above results. Overall, these computational data are consistent with the experimental trend and provide an interesting insight into the observed dissociate rates in these different heme protein systems.

## Supplementary figures and tables

**Table S1.** HCO type and the measured E° value of its catalytic heme

| CcO type and organism | Catalytic heme E°' | References |
|---|---|---|
| *R. sphaeroides cbb$_3$* oxidase | -59 mV (heme *b$_3$*) | [15] |

| | | |
|---|---|---|
| *E. coli bo$_3$ oxidase* | 160 mV to 200 mV (heme *o$_3$*) | [16]-[17] |
| *B. subtilis* PS3 caa$_3$ oxidase | 190 mV (heme *a$_3$*) | [18] |
| *T. thermophilus ba$_3$ oxidase* | 199 mV (heme *a$_3$*, pH 8.4) | [19] |
| *P. denitrificans caa$_3$ oxidase* | 220 mV (heme *a$_3$*) | [20] |
| *Bacillus* YN-2000 *aco* oxidase | 250 mV (heme *o$_3$*) | [21] |
| *B. pseudofirmus caa$_3$ oxidase* | 334 mV (heme *a$_3$*) | [22] |
| *A. ambivalens aa$_3$* oxidase | 390 ± 20 mV (heme *a$_3$*) | [23] |
| Bovine heart C*c*O | ~204 mV (heme *a$_3$*, low potential form)<br>~460 mV (heme *a$_3$*, high potential form) | **[24, 25]** |

**Table S2.** CO recombination rate constants at 1.5 mM CO.

*The data was fitted to one exponential, although some samples showed small contributions (in relative amplitude) of an additional faster phase

| **Sample** | $k_{obs}$ **(/s)*** |
|---|---|
| F33Y-Cu$_B$Mb | 0.7 |

| | |
|---|---|
| F33Y-S92A-$Cu_B$Mb | 2.3 |
| F33Y-$Cu_B$Mb (MF heme) | 3.1 |
| F33Y-$Cu_B$Mb (DF heme) | 14.8 |

**Table S3.** Key geometric parameters, charges, spin densities and energy data

| | $Fe\text{-}N_{His}$ | $Fe\text{-}O_2$ | $O_b\text{-}O_t$ | $\angle Fe\text{-}O_b\text{-}O_t$ | $\Delta E$ | $\Delta E_{ZPE}$ | $\Delta H$ | $\Delta G$ |
|---|---|---|---|---|---|---|---|---|
| | Å | Å | Å | degree | kcal/mol | kcal/mol | kcal/mol | kcal/mol |
| heme-b-$Fe^{2+}$-$O_2$ | 2.212 | 1.786 | 1.298 | 122.9 | 1.47 | 1.82 | 1.68 | 2.02 |
| heme-b-$Fe^{3+}$-$O_2^-$ | 2.204 | 1.852 | 1.301 | 121.5 | 0.00 | 0.00 | 0.00 | 0.00 |
| MF-heme-$Fe^{2+}$-$O_2$ | 2.207 | 1.788 | 1.297 | 122.9 | 1.40 | 1.75 | 1.61 | 1.99 |
| MF-heme-$Fe^{3+}$-$O_2^-$ | 2.200 | 1.851 | 1.300 | 121.5 | 0.00 | 0.00 | 0.00 | 0.00 |
| DF-heme-$Fe^{2+}$-$O_2$ | 2.203 | 1.788 | 1.296 | 122.9 | 1.42 | 1.78 | 1.63 | 2.01 |
| DF-heme-$Fe^{3+}$-$O_2^-$ | 2.197 | 1.852 | 1.298 | 121.5 | 0.00 | 0.00 | 0.00 | 0.00 |

| | Mulliken | | | | NPA | | | |
|---|---|---|---|---|---|---|---|---|
| | $Q_{Fe}$ | $Q_{Ob}$ | $Q_{Ot}$ | $Q_{O2}$ | $Q_{Fe}$ | $Q_{Ob}$ | $Q_{Ot}$ | $Q_{O2}$ |
| | e | e | e | e | e | e | e | e |
| heme-b-$Fe^{2+}$-$O_2$ | 1.950 | 0.072 | -0.123 | -0.051 | 0.417 | 0.011 | -0.215 | -0.203 |
| heme-b-$Fe^{3+}$-$O_2^-$ | 1.953 | -0.034 | -0.119 | -0.152 | 0.461 | -0.045 | -0.186 | -0.230 |
| MF-heme-$Fe^{2+}$-$O_2$ | 1.943 | 0.073 | -0.118 | -0.044 | 0.414 | 0.012 | -0.210 | -0.197 |
| MF-heme-$Fe^{3+}$-$O_2^-$ | 1.946 | -0.029 | -0.114 | -0.143 | 0.459 | -0.042 | -0.182 | -0.224 |
| DF-heme-$Fe^{2+}$-$O_2$ | 1.934 | 0.077 | -0.111 | -0.034 | 0.413 | 0.014 | -0.204 | -0.190 |
| DF-heme-$Fe^{3+}$-$O_2^-$ | 1.938 | -0.026 | -0.108 | -0.135 | 0.458 | -0.041 | -0.176 | -0.218 |

| | Mulliken | | | | NPA | | | |
|---|---|---|---|---|---|---|---|---|
| | $\rho_{\alpha\beta}^{Fe}$ | $\rho_{\alpha\beta}^{Ob}$ | $\rho_{\alpha\beta}^{Ot}$ | $\rho_{\alpha\beta}^{O2}$ | $\rho_{\alpha\beta}^{Fe}$ | $\rho_{\alpha\beta}^{Ob}$ | $\rho_{\alpha\beta}^{Ot}$ | $\rho_{\alpha\beta}^{O2}$ |
| | e | e | e | e | e | e | e | e |
| heme-b-$Fe^{2+}$-$O_2$ [a] | | | | | | | | |
| heme-b-$Fe^{3+}$-$O_2^-$ | -0.830 | 0.312 | 0.498 | 0.810 | -0.743 | 0.289 | 0.503 | 0.792 |
| MF-heme-$Fe^{2+}$-$O_2$ [a] | | | | | | | | |
| MF-heme-$Fe^{3+}$-$O_2^-$ | -0.820 | 0.305 | 0.493 | 0.799 | -0.734 | 0.282 | 0.498 | 0.780 |
| DF-heme-$Fe^{2+}$-$O_2$ [a] | | | | | | | | |
| DF-heme-$Fe^{3+}$-$O_2^-$ | 0.828 | -0.305 | -0.496 | -0.801 | 0.740 | -0.281 | -0.501 | -0.782 |

[a] For the oxy forms, spin densities are all zero.

**Table S4.** Variation of oxidase activity, ET rates, oxygen binding/dissociation rates with heme redox potential in F33Y-$Cu_B$Mb variants

| **E°' (mV)** | **$k_{cat}$ ($\mu Ms^{-1}$)** | **$k_{ET}$ ($s^{-1}$)** | **$k_{on}$ ($mM^{-1}$ $s^{-1}$)** | **$k_{off}$ ($s^{-1}$)** | **$K_D$ (mM)** |
|---|---|---|---|---|---|
| 95 ± 2 | 0.31 ± 0.01 | 0.10 ± 0.05 | 21 ± 2 | 14 ± 1 | 0.7 ± 0.08 |
| 123 ± 3 | 0.65 ± 0.08 | 0.19 ± 0.03 | 48 ± 3 | 11 ± 2 | 0.2 ±0.04 |
| 210 ± 6 | 1.49 ± 0.02 | 0.76 ± 0.02 | 70 ± 10 | 160 ± 10 | 2.3 ± 0.4 |
| 320 ± 10 | 2.06 ± 0.1 | 3.19 ± 0.07 | 250 ± 70 | 500 ± 40 | 2.0 ± 0.6 |

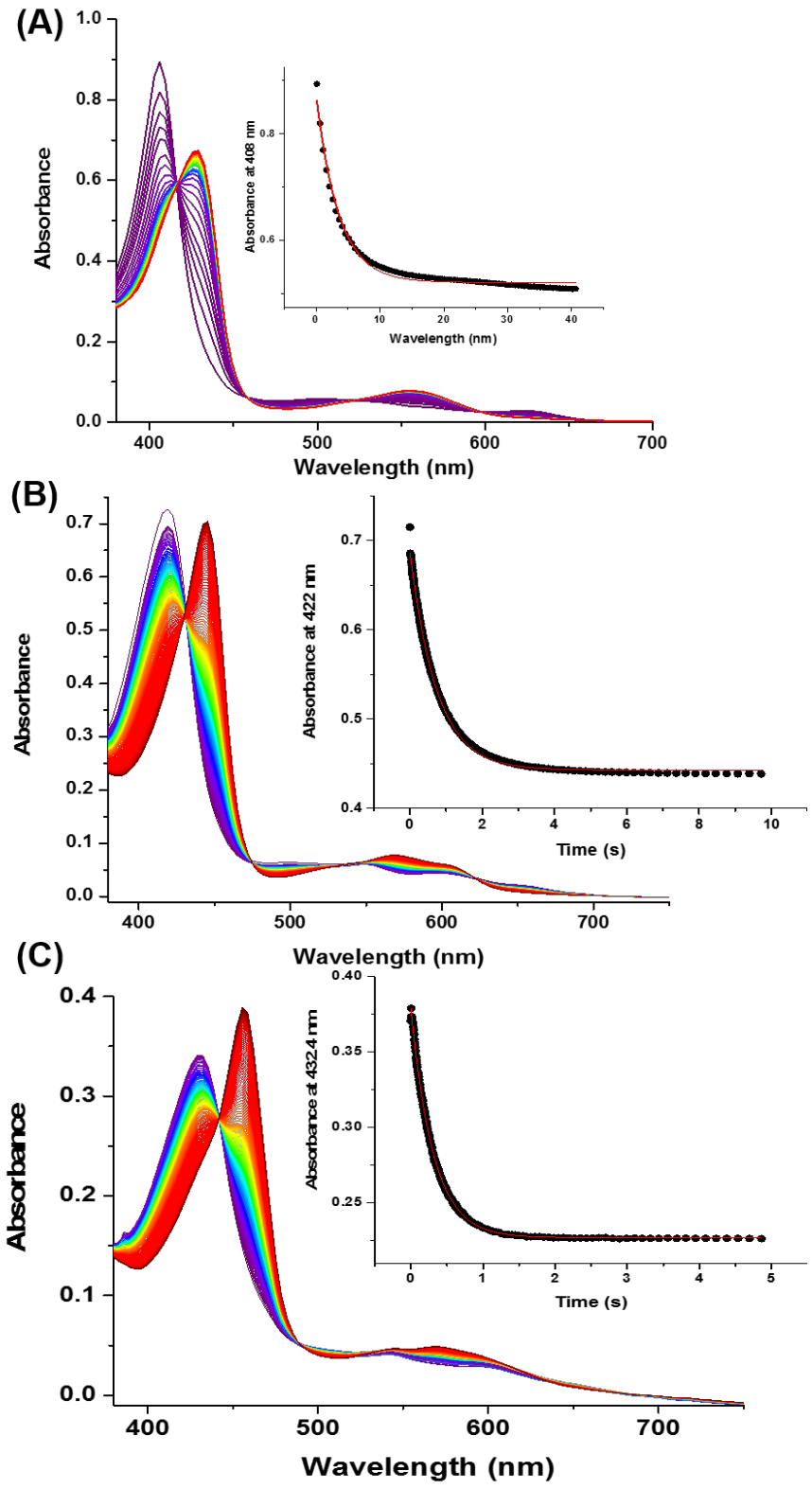


**Figure S1.** The stopped-flow UV-Vis measurements of the reaction between 6 μM of S92A-F33Y-Cu$_B$Mb (A), F33Y-Cu$_B$Mb (MF-heme) (B), F33Y-Cu$_B$Mb (DF-heme) (C) and 1 mM TMPD, 10 mM ascorbate between 0.001s to 100s. The spectra starts from ferric (violet) and goes to ferrous (maroon) form with clean isosbestic points. The inset shows the absorbance at $\lambda_{max}$ corresponding to Soret of ferric species.

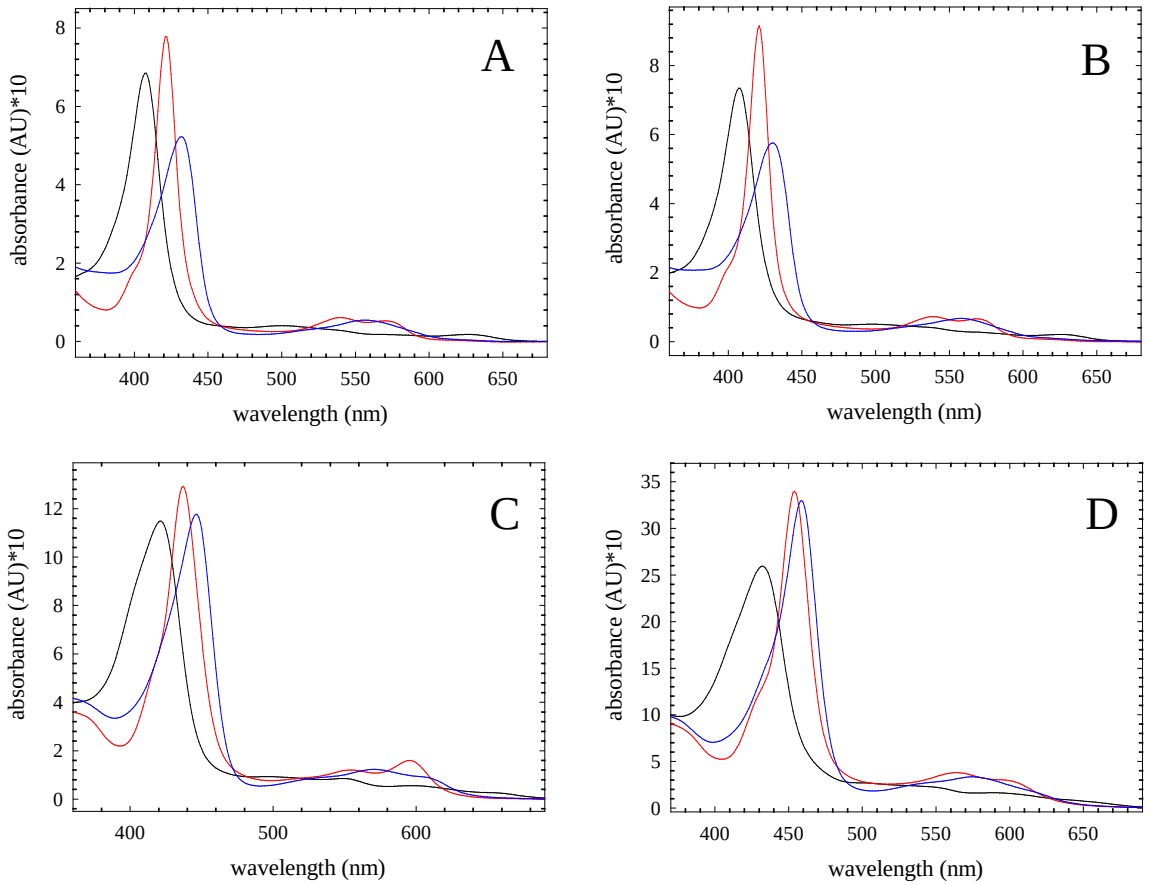


**Figure S2.** UV-Vis spectra of F33Y-$Cu_B$Mb (A), F33Y-S92A-$Cu_B$Mb (B), F33Y-$Cu_B$Mb (MF heme) (C), F33Y-$Cu_B$Mb (DF heme) (D). Ferric state under $N_2$ atmosphere (black trace), ferrous state (blue trace) and ferrous CO-bound state (red trace).

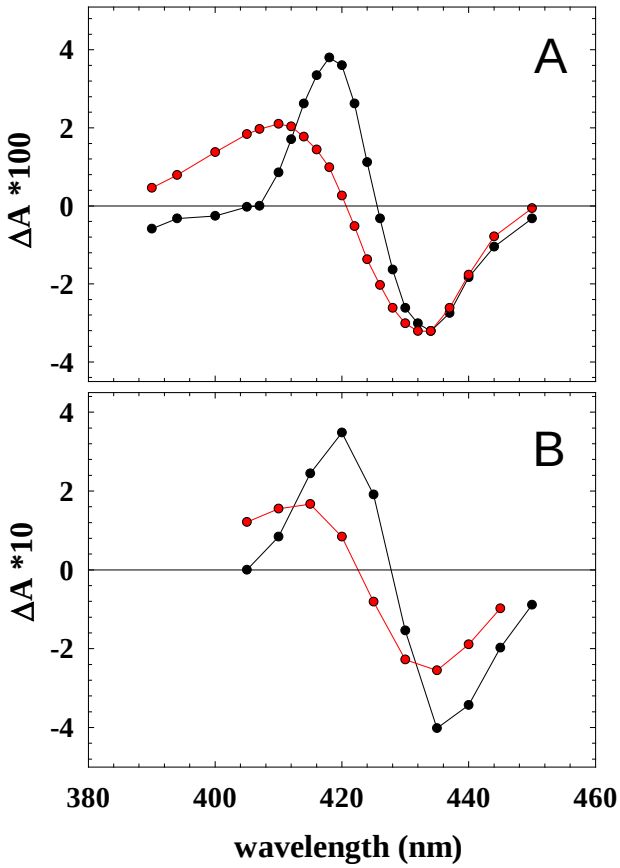


**Figure S3.** Kinetic difference spectra for wildtype Mb (A) and F33Y-$Cu_B$Mb (B). $O_2$ binding (red line) and CO binding (black line). Data for wildtype Mb were taken as in Flock *et. al.*[2] and from Verkovsky *et. al.*[26]

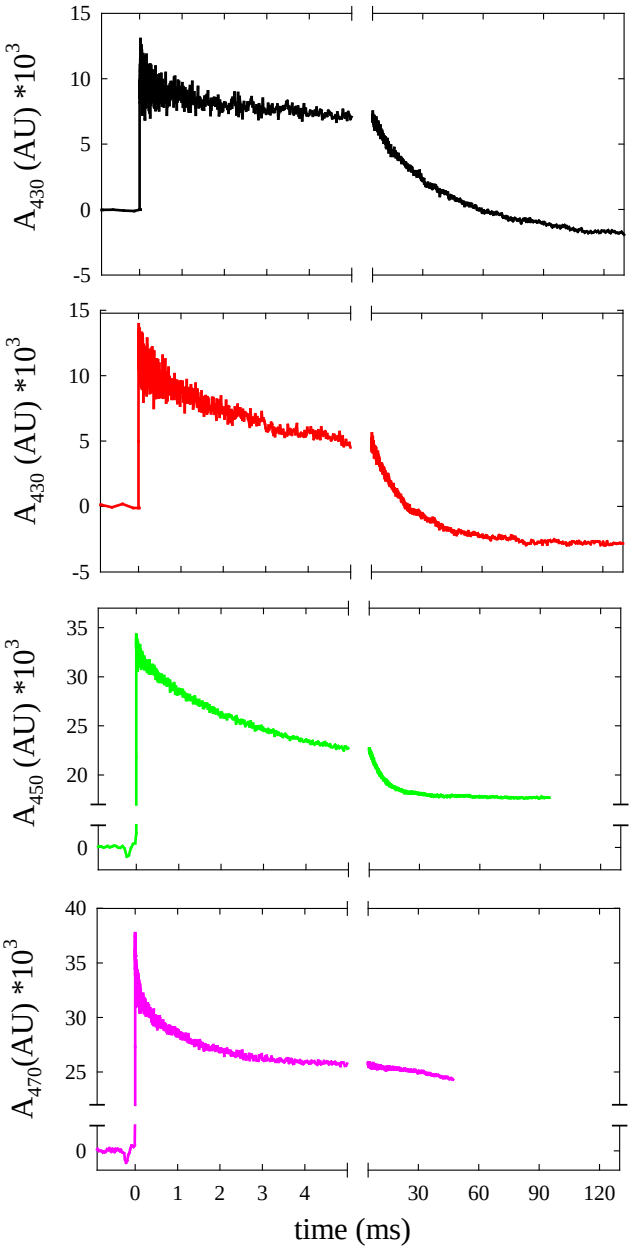


**Figure S4**. $O_2$ binding kinetics at 1 mM $O_2$. CO is dissociated at t = 0 ms. F33Y-$Cu_B$Mb (black), F33Y-S92A-$Cu_B$Mb (red), F33Y-$Cu_B$Mb MF (green), F33Y-$Cu_B$Mb DF (pink).

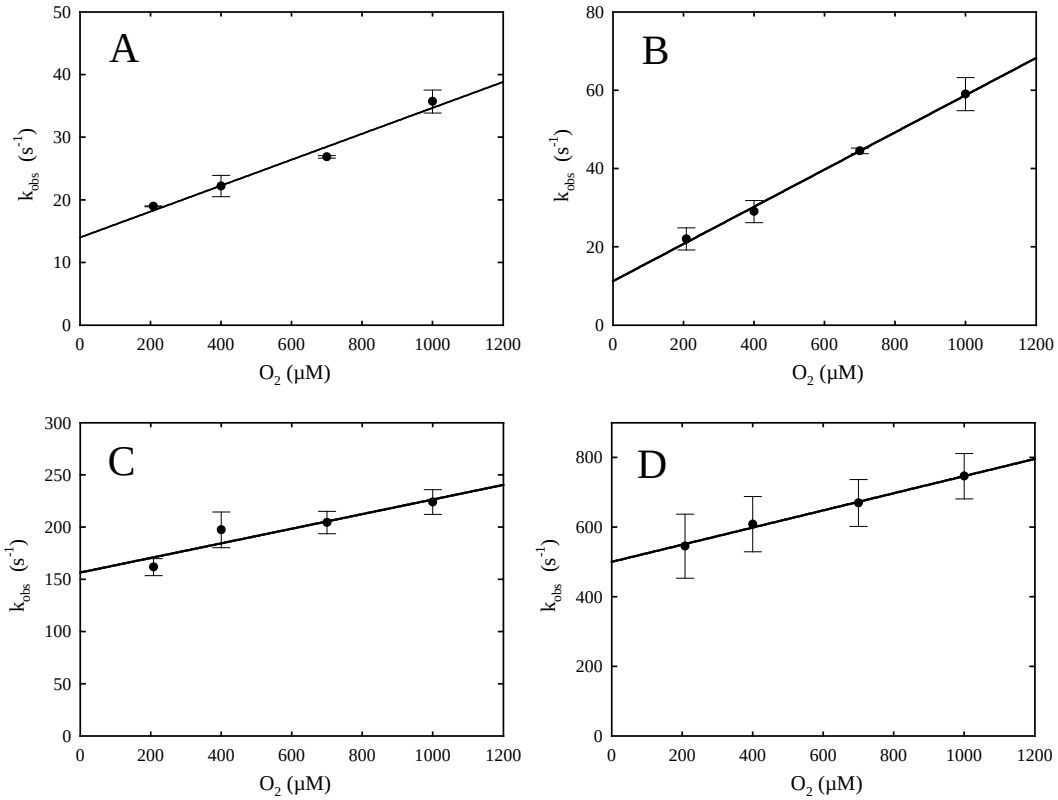


**Figure S5.** $O_2$ affinity measurements. The observed rate constant for $O_2$ binding is shown as function of the final $O_2$ concentration after mixing. Shown is the average and standard deviation. A: F33Y-$Cu_B$Mb (n=2), B: F33Y-S92A-$Cu_B$Mb (n=2), C: F33Y-$Cu_B$Mb MF (n=3), D: F33Y-$Cu_B$Mb DF (n=3).

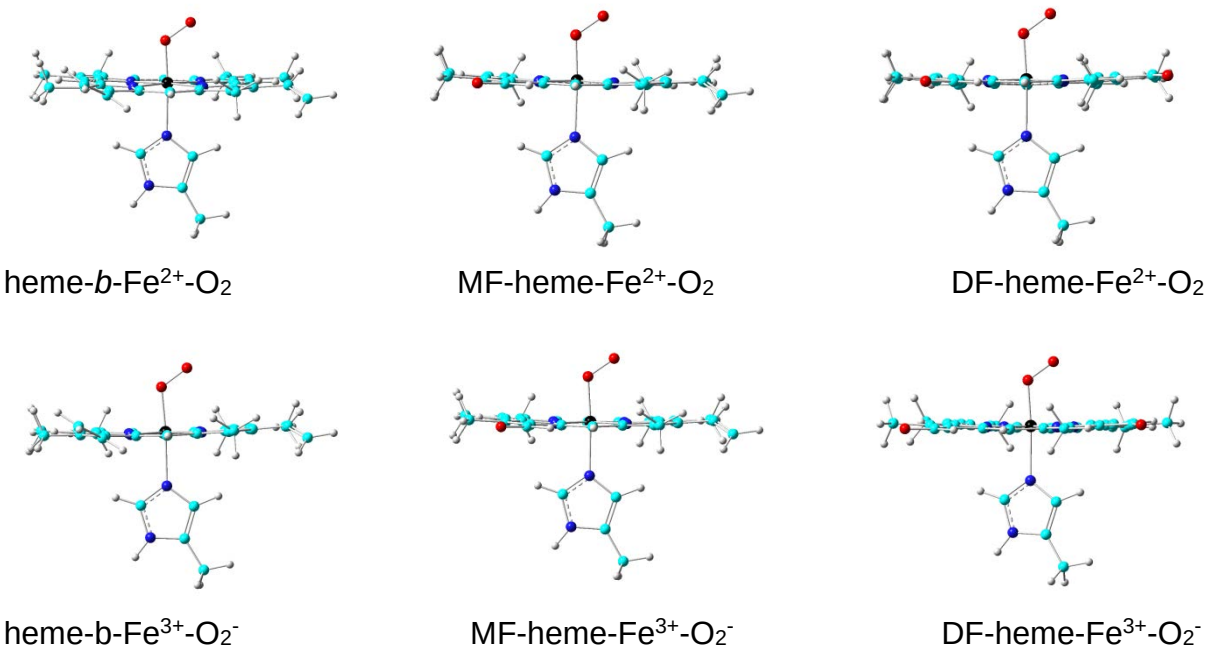


**Figure S6.** Optimized molecular structures

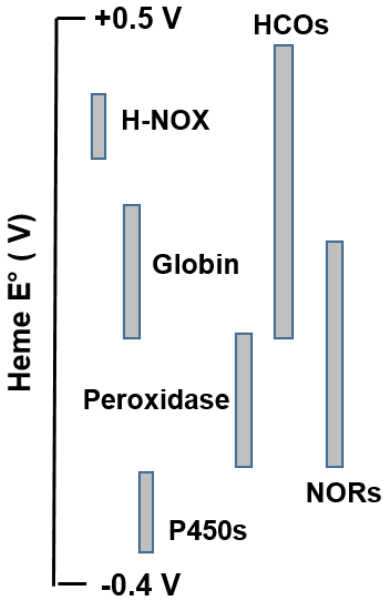


**Figure S7**. Heme E°’ of various heme proteins reported in literature[27, 28, 29]

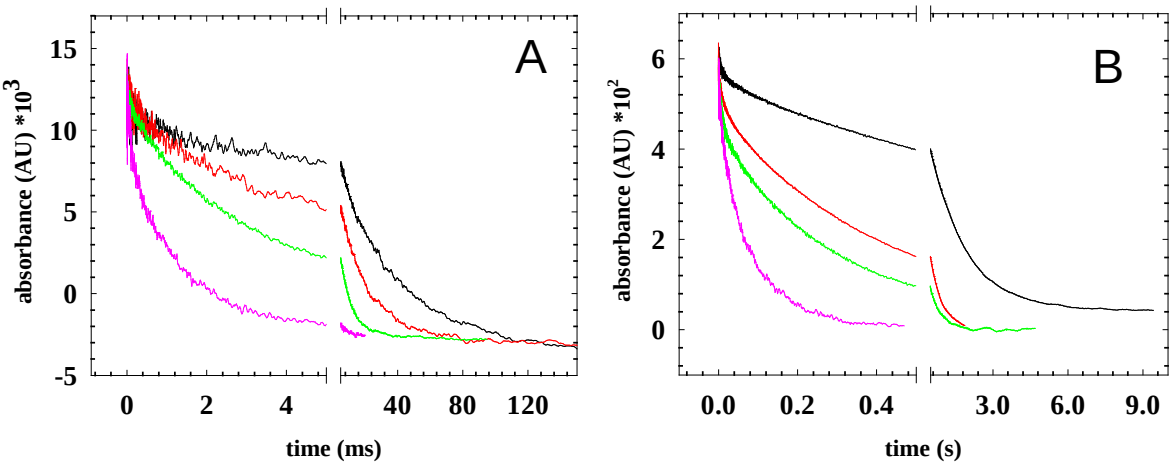


**Figure S8.** $O_2$ binding kinetics in Flow-Flash measurements at 1 mM $O_2$ (A) and CO recombination at 1.5 mM CO (B). F33Y-$Cu_B$Mb (black), F33Y-S92A-$Cu_B$Mb (red), F33Y-$Cu_B$Mb MF (green), F33Y-$Cu_B$Mb DF (pink). The data points have been averaged and the laser artifact at t~0 s has been removed for clarity reasons.

## References:


[1] A. Bhagi-Damodaran, I. D. Petrik, N. M. Marshall, H. Robinson, Y. Lu, *J. Am. Chem. Soc.* **2014**, *136*, 11882-11885.
[2] U. Flock, N. J. Watmough, P. Ädelroth, *Biochemistry* **2005**, *44*, 10711-10719.
[3] C. Adamo, V. Barone, *J. Chem. Phys.* **1998**, *108*, 664-675.
[4] S. H. Vosko, L. Wilk, M. Nusair, *Canadian Journal of Physics* **1980**, *58*, 1200-1211.
[5] A. J. Wachters, *J. Chem. Phys.* **1970**, *52*, 1033-1036.
[6] Y. Ling, C. Mills, R. Weber, L. Yang, Y. Zhang, *J. Am. Chem. Soc.* **2010**, *132*, 1583-1591.
[7] L. Yang, Y. Ling, Y. Zhang, *J. Am. Chem. Soc.* **2011**, *133*, 13814-13817.
[8] Frisch, M. J.; Trucks, G. W.; Schlegel, H. B.; Scuseria, G. E.; Robb, M. A.; Cheeseman, J. R.; Scalmani, G.; Barone, V.; Mennucci, B.; Petersson, G. A.; Nakatsuji, H.; Caricato, M.; Li, X.; Hratchian, H. P.; Izmaylov, A. F.; Bloino, J.; Zheng, G.; Sonnenberg, J. L.; Hada, M.; Ehara, M.; Toyota, K.; Fukuda, R.; Hasegawa, J.; Ishida, M.; Nakajima, T.; Honda, Y.; Kitao, O.; Nakai, H.; Vreven, T.; Montgomery, Jr., J. A.; J. Peralta, E.; Ogliaro, F.; Bearpark, M.; Heyd, J. J.; Brothers, E.; Kudin, K. N.; Staroverov, V. N.; Keith, T.; Kobayashi, R.; Normand,J.; Raghavachari, K.; Rendell, A.; Burant, J. C.; Iyengar, S. S.; Tomasi, J.; Cossi, M.; Rega, N.; Millam, J. M.; Klene, M.; Knox, J. E.; Cross, J. B.; Bakken, V.; Adamo, C.; Jaramillo, J.; Gomperts, R.; Stratmann, R. E.; Yazyev, O.; Austin, A. J.; Cammi, R.; Pomelli, C.; Ochterski, J. W.; Martin, R. L.; Morokuma, K.; Zakrzewski,V. G.; Voth, G. A.; Salvador, P.; Dannenberg, J. J.; Dapprich, S.; Daniels, A. D.; Farkas, O.; Foresman, J. B.; Ortiz, J. V.; Cioslowski, J.; Fox, D. J.; Gaussian 09, Revision D.01 ed., Gaussian, Inc., Wallingford CT, **2013**.
[9] H. Chen, M. Ikeda-Saito, S. Shaik, *J. Am. Chem. Soc.* **2008**, *130*, 14778-14790.
[10] L. M. Blomberg, M. R. A. Blomberg, P. E. M. Siegbahn, *J. Inorg. Biochem.* **2005**, *99*, 949-958.
[11] F. D. Angelis, A. A. Jarzecki, R. Car, T. G. Spiro, *J. Phys. Chem. B* **2005**, *109*, 3065-3070.
[12] E. Sigfridsson, U. Ryde, *J. Inorg. Biochem.* **2002**, *91*, 101-115.
[13] C. Rovira, K. Kunc, J. Hutter, P. Ballone, M. Parrinello, *Journal of Physical Chemistry A* **1997**, *101*, 8914-8925.
[14] Y. Ling, Y. Zhang, in *Annual Reports in Computational Chemistry, Vol. 6* (Ed.: R. A. Wheeler), Elsevier, New York, **2010**, pp. 65-77.
[15] V. Rauhamaki, D. A. Bloch, M. I. Verkhovsky, M. Wikström, *Journal of Biological Chemistry* **2009**, *284*, 11301-11308.
[16] J. C. Salerno, B. Bolgiano, W. J. Ingledew, *FEBS Letters* **1989**, *247*, 101-105.
[17] B. E. Schultz, S. I. Chan, *Proceedings of the National Academy of Sciences of the United States of America* **1998**, *95*, 11643-11648.
[18] R. K. Poole, *Biochim. Biophys. Acta, Rev. Bioenerg.* **1983**, *726*, 205-243.
[19] F. L. Sousa, A. F. Veríssimo, A. M. Baptista, T. Soulimane, M. Teixeira, M. M. Pereira, *Biophysical Journal* **2008**, *94*, 2434-2441.
[20] K. Pardhasaradhi, B. Ludwig, R. W. Hendler, *Biophysical Journal* **1991**, *60*, 408-414.
[21] Y. Orii, I. Yumoto, Y. Fukumori, T. Yamanaka, *J. Biol. Chem.* **1991**, *266*, 14310-14316.
[22] M. S. Muntyan, D. A. Bloch, *Biochemistry (Mosc)* **2008**, *73*, 107-111.
[23] S. Todorovic, M. M. Pereira, T. M. Bandeiras, M. Teixeira, P. Hildebrandt, D. H. Murgida, *J. Am. Chem. Soc.* **2005**, *127*, 13561-13566.
[24] R. W. Hendler, G. S. Sidhu, K. Pardhasaradhi, *Biophysical Journal* **1990**, *58*, 957-967.
[25] R. W. Hendler, G. S. Sidhu, *Biophysical Journal* **1988**, *54*, 121-133.
[26] M. I. Verkhovsky, J. E. Morgan, M. Wikstroem, *Biochemistry* **1994**, *33*, 3079-3086.
[27] C. Olea, Jr., J. Kuriyan, M. A. Marletta, *Journal of the American Chemical Society* **2010**, *132*, 12794-12795.
[28] C. H. Taboy, C. Bonaventura, A. L. Crumbliss, *Bioelectrochem. Bioenerg.* **1999**, *48*, 79-86.
[29] C. J. Reedy, M. M. Elvekrog, B. R. Gibney, *Nucleic Acids Research* **2008**, *36*, D307-D313.